Cyberspace: Jurnal Pendidikan Teknologi informasi
Volume 10, Nomor 1, April 2026, hal. 40 – 52
ISSN 2598-2079 (print) | ISSN 2597-9671 (online)

SIMULATION-DRIVEN METHOD FOR WATER COVERAGE MONITORING FROM MULTI-SENSOR SATELLITE IMAGERY

Andriani Putri*[1], Chih-Yuan Huang[2], Kuo-Hsin Tseng[3], Tang-Huang Lin[4], Hayatun Maghfirah[5], Sri Azizah Nazhifah[6], Abdurrahman Ridho[7], Cut Mutia[8]

[1,6]Departement of Informatics, Universitas Syiah Kuala, Banda Aceh, Indonesia
[2,3,4]Center for Space and Remote Sensing Research, National Central University, Taiwan
[5,7,8]Department of Information Technology, Universitas Teuku Umar, Aceh Barat, Indonesia
E-mail: [*1]andrianiputri@usk.ac.id, [2]cyhuang@csrsr.ncu.edu.tw, [3]khtseng@csrsr.ncu.edu.tw, [4]thlin@csrsr.ncu.edu.tw, [5]hayatunmaghfirah@utu.ac.id, [6]sriazizah07@unsyiah.ac.id, [7]abdurrahman.ridho@utu.ac.id, [8]cutmutia@utu.ac.id

Abstract

Monitoring water coverage in intertidal zones is challenging due to the lack of satellite sensors that simultaneously provide both high spatial and high temporal resolution. Landsat offers detailed spatial information but is limited by its 16-day revisit cycle, whereas Himawari-8 provides frequent observations but at coarse spatial scales. Existing multi-sensor fusion approaches, such as STARFM and ESTARFM, attempt to bridge this gap but rely on the assumption of linear or abrupt land cover changes, which is inadequate for capturing the gradual and non-linear dynamics of tidal environments. In this study, we propose a simulation-driven method for water coverage monitoring in intertidal zones by blending Landsat OLI and Himawari-8 imagery. The core innovation lies in simulating reference images that represent different water height conditions through interpolation of the Modified Normalized Difference Water Index (mNDWI) trends, with the objective of improving temporal continuity and capturing non-linear tidal dynamics more accurately. The approach integrates normalized Landsat OLI and Himawari-8 AHI imagery with digital elevation and tidal models to interpolate mNDWI values. Through linear interpolation, synthetic reference images are produced for low, medium, and high-water height scenarios, filling temporal gaps and providing additional input for fusion-based monitoring. Results from the Hsiang-Shan Wetland demonstrate that simulated reference images contribute more significantly to accurate water mapping than Himawari-8 data alone. The method improves temporal continuity, enhances the representation of tidal dynamics, and reduces discrepancies in fused outputs. Although the accuracy depends on DEM and tidal model quality, the findings highlight the potential of simulation-driven approaches to strengthen water monitoring frameworks. This method can be extended to support applications in flood mapping, wetland management, and coastal conservation.

Keywords: *simulation-driven, water coverage, multi-sensor satellite, linear interpolation*

Abstrak

Pemantauan cakupan air di zona intertidal merupakan tantangan karena tidak tersedianya sensor satelit yang secara simultan menyediakan resolusi spasial tinggi dan resolusi temporal tinggi. Landsat menawarkan informasi spasial yang rinci, namun terbatas oleh siklus kunjungan ulang selama 16 hari, sedangkan Himawari-8 menyediakan pengamatan yang sering tetapi pada skala spasial yang kasar. Pendekatan fusi multi-sensor yang ada, seperti STARFM dan ESTARFM, berupaya menjembatani kesenjangan ini, namun bergantung pada asumsi perubahan tutupan lahan yang bersifat linear atau mendadak, yang kurang memadai untuk menangkap dinamika lingkungan pasang surut yang bertahap dan non-linear. Dalam penelitian ini, kami mengusulkan metode berbasis simulasi untuk pemantauan cakupan air di zona intertidal dengan menggabungkan citra Landsat OLI dan Himawari-8. Inovasi utama terletak pada simulasi citra referensi yang merepresentasikan kondisi ketinggian air yang berbeda melalui interpolasi tren Modified Normalized Difference Water Index (mNDWI), dengan tujuan meningkatkan kontinuitas temporal dan menangkap dinamika pasang surut non-linear secara lebih akurat. Pendekatan ini mengintegrasikan citra Landsat OLI dan Himawari-8 AHI yang telah dinormalisasi dengan model elevasi digital dan model pasang surut untuk menginterpolasi nilai mNDWI. Melalui interpolasi linear, dihasilkan citra referensi sintetis untuk skenario ketinggian air rendah, sedang, dan tinggi, yang mengisi kekosongan temporal serta menyediakan masukan tambahan untuk pemantauan berbasis fusi. Hasil dari Lahan Basah Hsiang-Shan menunjukkan bahwa citra referensi hasil simulasi memberikan kontribusi yang lebih signifikan terhadap pemetaan air yang akurat dibandingkan dengan penggunaan data Himawari-8 saja. Metode ini meningkatkan kontinuitas temporal, memperkaya representasi dinamika pasang surut, serta mengurangi perbedaan pada hasil fusi. Meskipun tingkat akurasi bergantung pada kualitas model elevasi digital (DEM) dan model pasang surut, temuan ini menegaskan potensi pendekatan berbasis simulasi dalam memperkuat kerangka kerja pemantauan air. Metode ini juga dapat diperluas untuk mendukung aplikasi dalam pemetaan banjir, pengelolaan lahan basah, dan konservasi pesisir.

Kata kunci: *simulasi, cakupan air, satelit multi-sensor, interpolasi linear*

1. Introduction

Remote sensing has become a fundamental tool for monitoring dynamic environmental processes such as water coverage in coastal and intertidal zones [1], [2]. However, a persistent limitation remains: no single satellite sensor simultaneously provides high spatial and temporal resolution [3], [4]. For example, Landsat OLI provides 30 m spatial resolution but has a 16-day revisit cycle [5], while geostationary satellites such as Himawari-8 offer 10-minute observations at coarser spatial resolution [6].

To overcome this gap, multi-sensor data fusion has emerged as a promising strategy by combining the complementary strengths of different sensors. Methods such as the Spatial and Temporal Adaptive Reflectance Fusion Model (STARFM) [7], the Enhanced STARFM (ESTARFM) [8], and the Spatial Temporal Adaptive Algorithm for Mapping Reflectance Change (STAARCH) [9] have been widely applied. These approaches aim to predict fine-resolution images at high temporal frequencies by blending data from multiple sensors. However, their underlying assumptions introduce notable limitations. Most existing models, including ESTARFM and STAARCH, are primarily designed to handle linear or abrupt land cover changes, and therefore lack the capability to represent more complex transformation patterns. As a result, they cannot effectively capture other types of land cover dynamics, particularly those that are gradual and non-linear in nature. Such limitations reduce their applicability in dynamic coastal environments, where water coverage is influenced by complex, continuous, and non-linear processes such as tidal fluctuations.

This limitation highlights the need for alternative approaches that can better represent gradual water dynamics and address data gaps when high-quality observations are unavailable. One promising direction is the simulation of reference images to complement multi-sensor fusion [10]. By generating synthetic data using available observations, digital elevation models (DEM), and tidal models, it becomes possible to estimate water coverage conditions not directly captured by satellites. In this study, linear interpolation is adopted due to its simplicity and efficiency in modeling gradual, continuous tidal changes. These simulated images can then be integrated into fusion frameworks, reducing reliance on temporally sparse observations.

In this study, we propose a simulation-driven method for water coverage monitoring in intertidal zones by blending Landsat OLI and Himawari-8 imagery. The core innovation lies in simulating reference images that represent different water height conditions through interpolation of the Modified Normalized Difference Water Index (mNDWI) trends. The corresponding water height information is derived from the NAO.99b Tide Model, which provides continuous tidal predictions to support the simulation process. Landsat OLI is selected due to its radiometric consistency, longer historical record, and more stable spectral characteristics, which are essential for reliable multi-temporal analysis and integration with Himawari-8 data. In addition, the spectral band configuration of Landsat OLI is widely validated for water index calculations such as mNDWI, making it more suitable for this study's simulation framework. By doing so, the method addresses the shortcomings of conventional fusion models and enhances the accuracy and continuity of water coverage monitoring in dynamic coastal wetlands. Specifically, this research aims to: (1) develop a simulation framework for generating reference images at varying water height levels, (2) integrate the simulated data into a fusion-based monitoring approach, and (3) evaluate the effectiveness of the proposed method across low, medium, and high-water height scenarios in the Hsiang-Shan Wetland.

2. Research Method

The methodology of this study is structured around the integration of multi-source satellite imagery, hydrological models, and simulation-based approaches to monitor water coverage dynamics in tidal wetlands. The overall workflow (Fig.1) consists of five main stages: data input, water index calculation, simulation of reference images, fusion using STARFM, and evaluation.

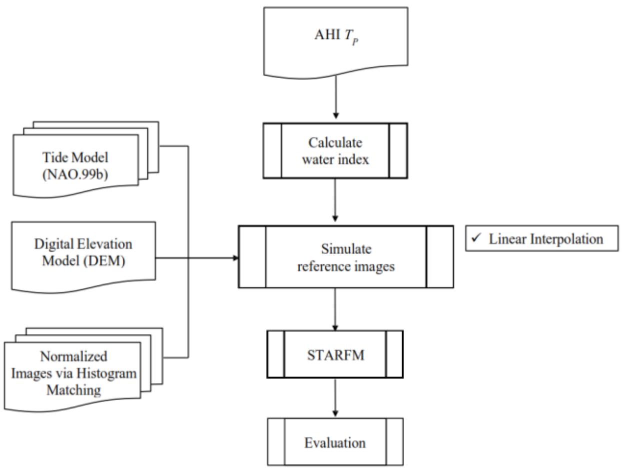

Figure 1. The overall workflow

The research was conducted in the Hsiang-Shan Wetland as shown in Fig. 2, a coastal wetland system characterized by significant fluctuations in water coverage due to tidal variation and seasonal hydrological dynamics. This wetland was selected because of its ecological importance and the pronounced influence of tidal cycles on its surface water extent.

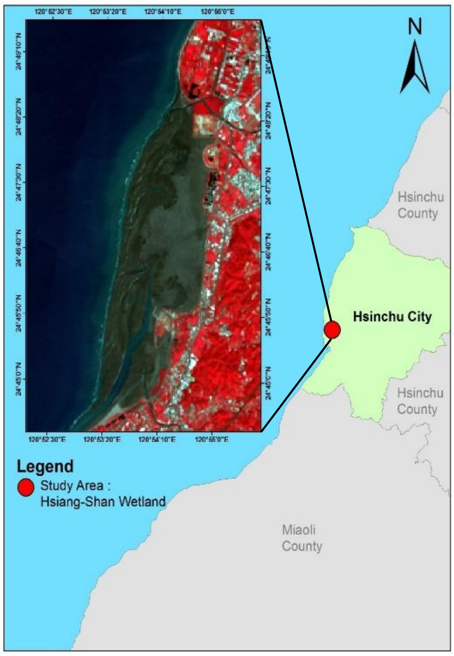

Figure 2. The area of study

To achieve this objective, two complementary satellite datasets were employed. The primary source of high-resolution imagery used in this study was the Landsat 8 Operational Land Imager (OLI). Landsat 8 OLI is a widely recognized sensor in earth observation studies due to its ability to provide consistent multispectral data with a spatial resolution of 30 meters. This resolution makes it highly effective for identifying small- to medium-scale hydrological features, including rivers, ponds, wetlands, and coastal water boundaries. In terms of revisit cycle, Landsat imagery has a temporal resolution of approximately 16 days, which is sufficient for monitoring seasonal and long-term land cover changes but insufficient for capturing rapid or short-lived hydrological dynamics such as tidal fluctuations, storm surges, or sudden flood events. In this research, the Green band (0.53–0.59 μm) and the Shortwave Infrared (SWIR1, 1.57–1.65 μm) band were specifically utilized to calculate the Modified Normalized Difference Water Index (mNDWI), which enhances open water bodies and reduces interference from vegetation or built-up areas. While Landsat OLI provides the spatial precision necessary to delineate fine water boundaries, its long revisit period makes it less suitable for continuous monitoring in highly dynamic environments.

To complement the spatial strengths of Landsat, Himawari-8 Advanced Himawari Imager (AHI) data was incorporated into the study. The Himawari-8 satellite, operated by the Japan Meteorological Agency, is designed primarily for meteorological monitoring but has also proven valuable for environmental studies requiring frequent temporal observations. The AHI sensor offers exceptional temporal resolution by capturing imagery every 10 minutes across the Asia-Pacific region, thus enabling near-continuous tracking of short-term environmental processes. However, this advantage comes at the cost of relatively coarse spatial resolution, ranging from approximately 500 meters to 2 kilometers depending on the spectral band used. While the coarse resolution limits its ability to detect fine-scale water bodies or narrow streams, the high frequency of AHI acquisitions makes it highly suitable for identifying rapid hydrological variations such as tidal ebb and flow, diurnal water level changes, and other transient events. By combining AHI with Landsat OLI, it is possible to achieve both temporal continuity and spatial detail in surface water monitoring, addressing the inherent limitations of each individual dataset.

In addition to satellite imagery, two ancillary datasets were employed to improve water coverage assessment and strengthen the simulation framework. The first was the Digital Elevation Model (DEM) of the Hsiang-Shan Wetland [11], which provides detailed elevation and terrain characteristics essential for estimating water height (WH). DEM data is particularly valuable in coastal wetland studies because it allows researchers to correlate observed water extents with underlying topography and predict inundation patterns at varying tidal levels. The second ancillary dataset was the NAO.99b Tide Model, a global ocean tide model that provides tidal predictions for the study period. This model was used to generate reference values of water height, which were later incorporated into the simulation of reference images. The integration of Landsat OLI, Himawari-8 AHI, DEM, and the NAO.99b Tide Model formed a robust multi-source dataset that enabled a more comprehensive and reliable assessment of water coverage dynamics. By combining high spatial detail, high temporal frequency, and physically meaningful topographic and tidal information, this approach overcomes the shortcomings of relying on a single data source and ensures more accurate.

2.1 Data Prepocessing

The first step in the preprocessing workflow involved the calculation of the Modified Normalized Difference Water Index (mNDWI), which was developed by [12] as an enhancement of the traditional NDWI. The mNDWI was selected because of its proven effectiveness in detecting open water bodies while minimizing spectral confusion with surrounding land features such as vegetation, bare soil, or urban structures. Unlike indices that rely heavily on near-infrared bands, mNDWI substitutes the near-infrared band with the shortwave infrared (SWIR) band, resulting in higher contrast between water and non-water surfaces. The index was calculated as (1):

$$mNDWI = \frac{GREEN - MIR}{GREEN + MIR} \qquad (1)$$

The Green band corresponds to wavelengths between 0.53–0.59 µm and the SWIR1 band corresponds to 1.57–1.65 µm. By emphasizing water's strong absorption in the SWIR region and relatively high reflectance in the green region, this formulation enhances the spectral signature of water. After the index was computed, a classification threshold was applied: pixels with mNDWI >0.4 were designated as water, while those below the threshold were considered non-water. The threshold value of 0.4 was not arbitrarily chosen; it was derived from empirical tests conducted within the study area and supported by previous wetland studies [11], which demonstrated its robustness in differentiating water surfaces under variable environmental conditions.

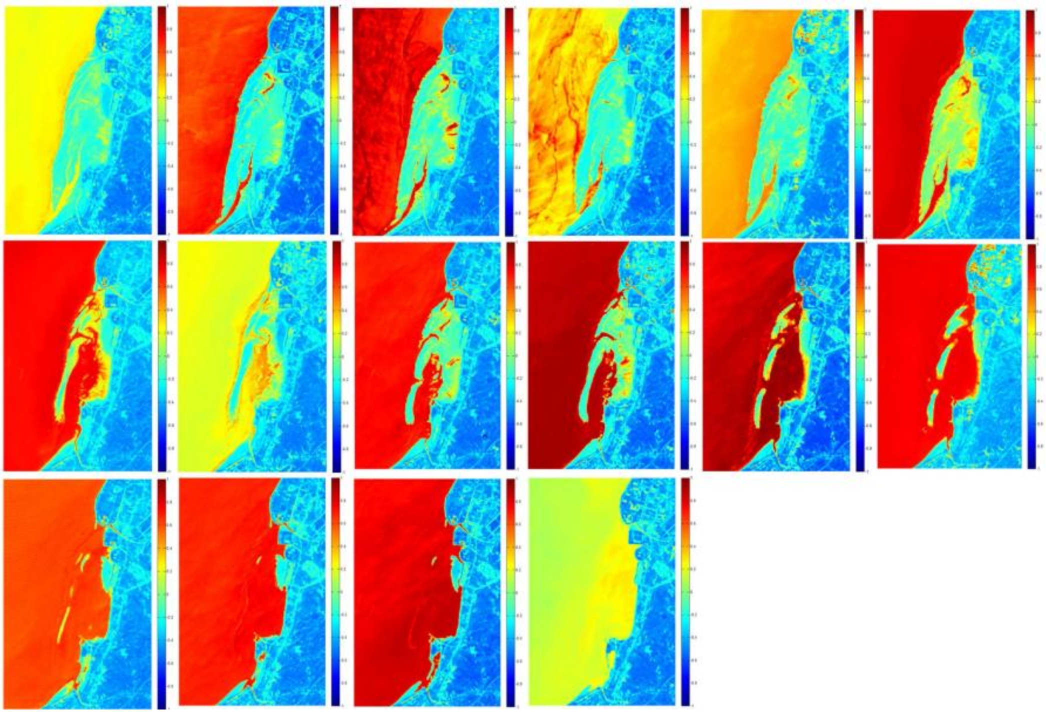

Figure 3. The mNDWI images of Landsat

The images in Fig. 3 represent tidal conditions from low tide to high tide, corresponding to increasing water heights. They illustrate varying water height conditions, with Table 1 listing the corresponding water height values in ascending order. The mNDWI values range from −1 to 1, where lower water levels are dominated by non-water pixels, while higher water levels indicate an increased presence of water pixels.

TABLE 2. WATER HEIGHTS (M) FROM LOWEST TO HIGHEST

No	Date	Water Height(m)
1	16/08/2015	-1.604
2	11/10/2016	-1.595
3	30/06/2016	-1.405
4	1/9/2016	-1.246
5	2/5/2016	-1.15
6	23/12/2016	-0.932
7	19/10/2015	0.216
8	10/4/2015	0.412
9	13/02/2015	0.516
10	26/01/2016	0.525
11	14/12/2016	0.748
12	16/10/2015	0.926
13	30/03/2016	1.369
14	22/12/2015	1.468
15	3/12/2016	1.6
16	23/07/2016	1.724

Despite the effectiveness of mNDWI, it is well understood that sensor-specific radiometric differences can introduce inconsistencies when comparing datasets across platforms. For example, Landsat 8 OLI and Himawari-8 AHI differ not only in their spatial and temporal resolution but also in their radiometric calibration, atmospheric influence, and spectral response functions. As a result, the raw mNDWI values calculated from these two sensors are not directly comparable.

2.2 Simulation Strategy for Reference Image Generation

The simulation process was carried out in three main steps. First, all Landsat and Himawari-8 derived mNDWI values underwent normalization via histogram matching, ensuring radiometric consistency across platforms and acquisition times. This step was essential to reduce sensor-related discrepancies and place both datasets into a comparable range. Second, mNDWI trends were extracted in relation to Digital Elevation Model (DEM)–derived water height (WH) conditions. By linking observed mNDWI values to corresponding water heights, the study established a physically meaningful relationship between tidal stage and water coverage extent. This relationship served as the foundation for predicting water distributions under unobserved tidal conditions. Finally, a linear interpolation method was applied to generate synthetic images corresponding to intermediate water height conditions. This interpolation estimated mNDWI values by using two temporally or hydrologically adjacent reference images as anchors, effectively producing new images that mimicked actual satellite observations.

As illustrated in Fig. 4, the interpolation assumes that the change in mNDWI values between two observed water heights is approximately linear. The interpolation method applied in this study follows the principle of linear interpolation, which estimates unknown values between two known reference points as shown in (3).

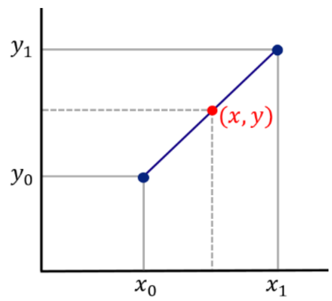

Figure 4. The illustration of linear interpolation

In the context of this research, the known reference points are the average mNDWI values (y_1 and y_0) corresponding to two distinct water heights (x_1 and x_0) derived from DEM and tidal model data. The objective is to generate a simulated mNDWI value (y) for an intermediate water height (x) where no direct observation is available. The formula used to estimate the intermediate value is expressed as:

$$y = \frac{y_1 - y_0}{x_1 - x_0} (x - x_0) + y_0 \qquad (3)$$

In this equation, (x_0, y_0) and (x_1 , y_1) represent the anchor points obtained from observed datasets, while (x , y) denotes the interpolated point. The red marker in the figure shows the estimated value at an intermediate condition, calculated as a weighted proportion of the distances between the two known points. This interpolation technique was applied repeatedly across pixels and water height conditions to generate complete synthetic reference images.

2.3 Spatial and Temporal Image Fusion

Simulated images were incorporated into a STARFM-inspired fusion model. By combining observed and simulated reference data, the method generates synthetic Landsat-like observations at varying tidal stages, improving monitoring continuity and accuracy.

Using a single pixel to predict reflectance would be easily affected by noises due to the changing reflectance based on the land cover types. Therefore, the Equation 3 was adjusted to the heterogeneous pixels. By adding more information from the neighboring pixels, STARFM try to address this issue and can be expressed in (4).

$$F(x_{w/2}, y_{w/2}, t_p) = \Sigma_i^w \Sigma_j^w \; W_{ijk} \times (\, C(x_i, y_j, t_p) - C(x_i, y_j, t_0) + F(x_i, y_j, t_0)\,) \tag{4}$$

The parameter w denotes the size of the moving search window, while $(x_{w/2}, y_{w/2})$represents the central pixel within that window. The symbols F and C correspond to the fine-resolution and coarse-resolution images, respectively. The variables $t_0$and $t_p$indicate the acquisition times of the reference image and the prediction image. The weighting factor W is determined by integrating spectral similarity, temporal proximity, and spatial distance information. To ensure reliable prediction, only spectrally similar and cloud-free Landsat surface reflectance pixels within the defined moving window are considered. The final predicted reflectance value is calculated as a weighted combination of these selected neighboring pixels. Specifically, the weight W_{ijk}quantifies the contribution of each neighboring pixel to the reflectance estimation of the central pixel.

3. Results and Discussion

To rigorously evaluate the effectiveness of the proposed simulation-driven approach, three representative tidal conditions were selected: low water height (–1.595 m, acquired on 11/10/2016), medium water height (0.216 m, acquired on 19/10/2015), and high-water height (1.724 m, acquired on 23/07/2016). These conditions capture the full range of tidal variability, from extreme ebb to peak inundation, and thus provide a robust basis for evaluating model performance under different hydrodynamic scenarios.

The significance of this simulation approach extends beyond simple data augmentation. By producing synthetic reference maps, the method addressed one of the most persistent limitations in remote sensing of wetlands: the inability of existing fusion models to capture gradual, non-linear, or cyclical changes in land cover. Whereas traditional models such as STARFM and ESTARFM assume either linear reflectance changes or sudden transitions, the simulation-driven method incorporated hydrological dynamics explicitly through DEM–WH information. As a result, the synthetic images not only filled data gaps but also improved the realism and accuracy of the fusion process. The original mNDWI images corresponding to each water height were used to evaluate both the simulated and predicted results. All original images are presented in Fig. 5. Specifically, Fig. 5(a) shows the original mNDWI image for low water levels, Fig. 5(b) represents the middle water height condition, and Figure 5(c) illustrates the high-water level condition.

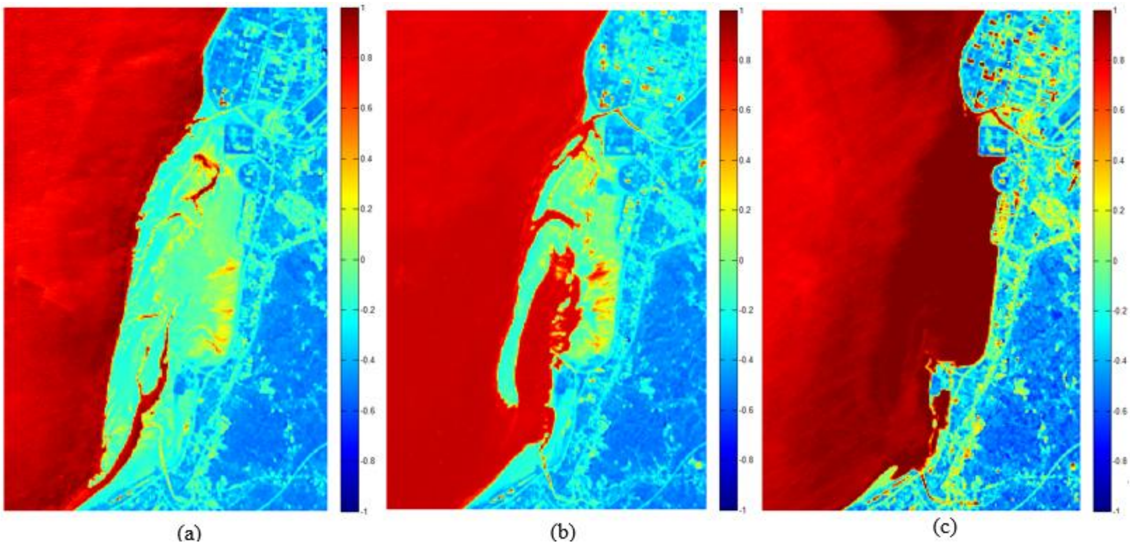

Figure 5. The original mNDWI images for different water heights. (a) The $Original\ Ft_p$ of low water height; (b) The $Original\ Ft_p$ of middle water height; (c) The $Original\ Ft_p$ of high-water height

Fig. 6 illustrates the simulated results for different water heights. The simulations were generated using an interpolation method based on the preceding and subsequent reference images. Fig. 6(a) presents the simulated result for low water heights, showing a greater proportion of non-water pixels within the study area. The simulated image for middle water height is shown in Fig. 6(b), where the number of water pixels slightly increases. In contrast, Fig. 6(c) depicts the simulation result for high water height, characterized by a substantially larger proportion of water pixels.

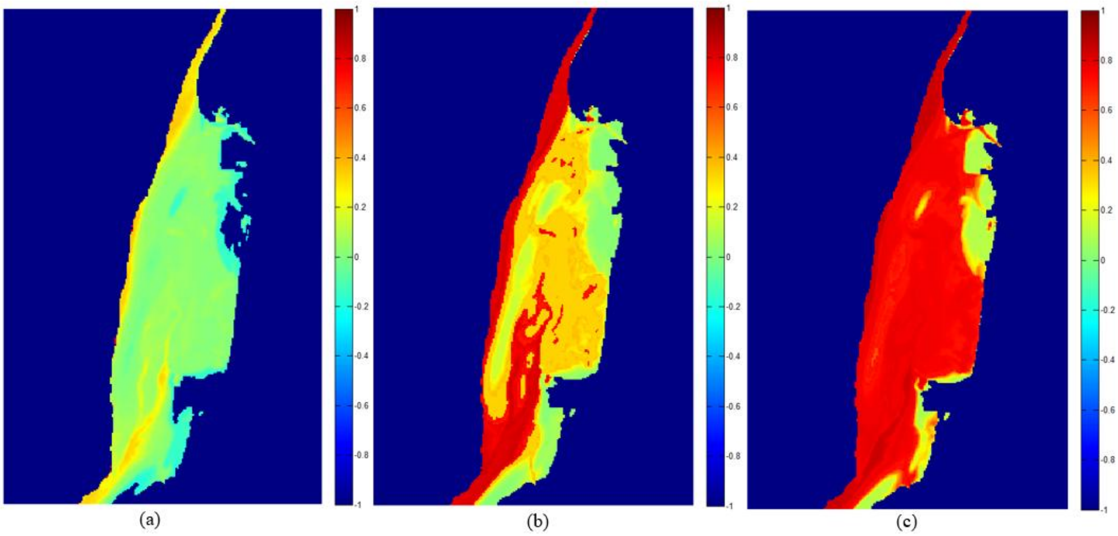

Figure 6. The simulated results for different water heights. (a) The $Simulated\ Ft_p$ of low water height; (b) The $Simulated\ Ft_p$ of middle water height; (c) The $Simulated\ Ft_p$ of high-water height

After generating the simulated images, the next step was to predict the fused images. This prediction was performed by integrating images acquired from two different sensors using the ESTARFM method, as illustrated in Fig. 7. Fig. 7(a) presents the predicted image for low water height. The predicted result for middle water height is shown in Fig. 7(b), while Fig. 7(c) displays the predicted image for high water height.

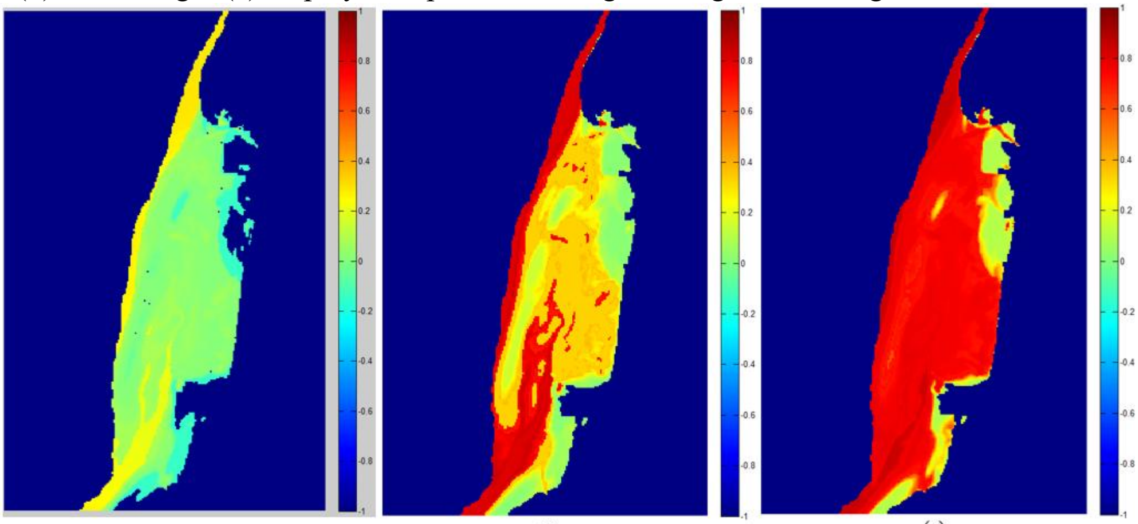

Figure 7. The Predicted results for different water heights. (a) The $Predicted\ Ft_p$ of low water height; (b) The $Predicted\ Ft_p$ of middle water height; (c) The $Predicted\ Ft_p$ of high-water height

For evaluation purposes, several spatial accuracy metrics were employed, including commission error, omission error, overall accuracy, and the Kappa coefficient. These metrics were used to assess the reliability of the simulated images relative to the reference images and to determine their potential applicability in addressing limitations in spatial image availability. To evaluate both the simulated and predicted results, the water maps derived from each image were first overlaid with the corresponding original images. Subsequently, the accuracy metrics were calculated based on the resulting comparison as shown in Table 2.

TABLE 2. THE EVALUATION RESULTS

No.	Image Category	WH Case	Commission error (%)	Omission error (%)	Overall accuracy (%)	Kappa Coefficient
1	Simulated Image	Low	5.21	2.30	72.32	0.71
		Middle	2.10	6.32	73.2	0.71
		High	0.79	4.53	82.42	0.77
2	Fused Image	Low	5.65	2.40	72.10	0.71
		Middle	1.93	6.02	76	0.73
		High	0.56	4.12	83.67	0.79

Table 2 presents the spatial accuracy assessment results for both the simulated and fused images under three water height (WH) conditions: low, middle, and high. In general, the results indicate that classification performance improves as the water level increases. For the simulated images, the commission error decreases substantially from 5.21% (low water height) to 0.79% (high water height), indicating a reduction in false positive water classifications at higher water levels. Although the omission error fluctuates across the three water heights, the overall accuracy increases from 72.32% (low) and 73.20% (middle) to 82.42% (high). Similarly, the Kappa coefficient improves from 0.71 to 0.77, suggesting a stronger agreement between the simulated results and the reference images under high water conditions.

A comparable pattern is observed for the fused images. The commission error declines from 5.65% (low) to 0.56% (high), while the overall accuracy increases from 72.10% to 83.67%. The Kappa coefficient also improves from 0.71 (low) to 0.79 (high), indicating substantial agreement in the high-water level scenario. Notably, the fused images consistently achieve slightly higher overall accuracy and Kappa values than the simulated images, particularly under middle and high-water conditions.

Importantly, the performance of the simulated images—achieving overall accuracy above 72% and Kappa values greater than 0.70 across all water height conditions—demonstrates that the simulation approach provides reasonably reliable results. This finding suggests that image simulation can serve as a practical alternative when reference images are limited or unavailable due to temporal gaps, cloud cover, or sensor constraints. Therefore, the simulation method offers a viable solution to mitigate the limitations of reference image availability in water body monitoring applications.

These findings suggest that both simulation and fusion approaches are more reliable in detecting water bodies during high water heights, where the spatial extent of water is more distinct. Furthermore, the superior performance of the fused images demonstrates the effectiveness of multi-sensor integration using STARFM in enhancing classification accuracy and mitigating the limitations of spatial image availability.

4. Conclusion

This study proposed a simulation-driven method to enhance water coverage monitoring in dynamic intertidal environments by integrating multi-sensor satellite imagery with digital elevation and tidal models. By generating synthetic reference images through linear interpolation of mNDWI values under different water height conditions, the proposed framework addressed a fundamental limitation in remote sensing applications: the lack of satellite data that simultaneously provides high spatial and high temporal resolution. The integration of Landsat 8 OLI, Himawari-8 AHI, DEM data, and tidal modeling enabled a more comprehensive representation of tidal dynamics in the Hsiang-Shan Wetland.

The evaluation results demonstrated that both simulated and fused images achieved satisfactory classification performance, with overall accuracy exceeding 72% and Kappa coefficients above 0.70 across all water height conditions. Notably, accuracy improved under high water conditions, indicating that the method effectively captures distinct inundation patterns. Furthermore, fused images generated using STARFM consistently outperformed standalone simulated images, confirming the benefit of multi-sensor integration. Importantly, the relatively strong performance of the simulated images highlights their potential as an alternative reference source when cloud cover, revisit limitations, or data gaps restrict the availability of high-quality observations.

Beyond improving classification accuracy, the simulation-driven approach contributes conceptually by incorporating hydrological constraints into the fusion process, thereby overcoming the limitations of conventional models that assume linear or abrupt land cover changes. Although the framework's performance depends on the quality of DEM and tidal data, the results indicate strong potential for broader applications. The proposed method can support continuous water monitoring, flood assessment, wetland management, and coastal conservation planning in data-scarce or highly dynamic environments.

References

[1] X. Xu, J. Li, H. Zhao, and Y. Wang, "Remote sensing of surface water dynamics in coastal and intertidal environments: A review," *Remote Sensing of Environment*, vol. 271, p. 112897, 2022.

[2] C. Donchyts, J. Schellekens, H. Winsemius, E. Eisemann, and H. Savenije, "Global surface water dynamics derived from satellite observations," *Nature Climate Change*, vol. 6, pp. 810–813, 2016.

[3] X. Zhu, F. Cai, J. Tian, and T. Williams, "Spatiotemporal fusion of multisource remote sensing data: Literature survey, taxonomy, principles, applications, and future directions," *Remote Sensing of Environment*, vol. 160, pp. 360–384, 2015.

[4] Y. Zhu, X. Xu, X. Wang, and L. Li, "Deep learning based spatiotemporal fusion in remote sensing: A comprehensive review," *IEEE Journal of Selected Topics in Applied Earth Observations and Remote Sensing*, vol. 16, pp. 1–24, 2023.

[5] J. R. Irons, J. L. Dwyer, and J. A. Barsi, "The next Landsat satellite: The Landsat Data Continuity Mission," *Remote Sensing of Environment*, vol. 122, pp. 11–21, 2012.*arth Observations and Remote Sensing*, vol. 16, pp. 1–24, 2023.

[6] T. Bessho *et al.*, "An introduction to Himawari-8/9—Japan's new-generation geostationary meteorological satellites," *Journal of the Meteorological Society of Japan*, vol. 94, no. 2, pp. 151–183, 2016.

[7] C. Gao, J. W. Masek, C. D. Kinker, E. F. Vermote, N. E. Zoltan, and Z. Zhu, "On the blending of the Landsat and MODIS surface reflectance: Predicting daily Landsat surface reflectance," *IEEE Transactions on Geoscience and Remote Sensing*, vol. 44, no. 8, pp. 2207–2218, Aug. 2006.

[8] X. Zhu, C. D. Elvidge, C. M. Tuttle, and C. Milloy, "An enhanced spatial and temporal adaptive reflectance fusion model (ESTARFM) for generating high-resolution image time series," *Remote Sensing of Environment*, vol. 114, no. 1, pp. 261–277, Jan. 2010.

[9] S. Hilker, M. R. Halligan, A. R. Townsend, P. C. Bolstad, and P. V. Bolstad, "Spatial Temporal Adaptive Algorithm for Mapping Reflectance Change (STAARCH) using Landsat imagery," *Remote Sensing of Environment*, vol. 113, no. 7, pp. 1416–1430, Jul. 2009.

[10] L. Zhu *et al.*, "Simulating fine spatial resolution imagery from coarse resolution data using generative adversarial networks," *Remote Sensing*, vol. 12, no. 18, p. 2932, 2020.

[11] K. H. Tseng, C. Y. Kuo, T. H. Lin, Z. C. Huang, Y. C. Lin, W. H. Liao, and C. F. Chen, "Reconstruction of time-varying tidal flat topography using optical remote sensing imageries," *ISPRS Journal of Photogrammetry and Remote Sensing*, vol. 131, pp. 92–103, 2017.

[12] H. Xu, "Modification of normalised difference water index (NDWI) to enhance open water features in remotely sensed imagery," *International Journal of Remote Sensing*, vol. 27, no. 14, pp. 3025–3033, 2006